

# A multifunctional quantum thermal device: with and without inner coupling

Yong Huangfu,<sup>1</sup> Shifan Qi,<sup>1</sup> and Jun Jing<sup>1,\*</sup>

<sup>1</sup>*Department of Physics, Zhejiang University, Hangzhou 310027, Zhejiang, China*

(Dated: August 31, 2020)

Quantum thermal devices have attracted growing attentions since they can be used to manipulate the heat currents of macroscopic thermal baths in a microscopic scale. In the present work, a three-level system attached to three thermal baths with different temperatures is exploited to serve as a valve, a refrigerator, an amplifier, and a thermometer in the quantum regime, via tuning the inner coupling strength of the system and the temperatures of the external baths. We discuss the connections among these thermal functions in the steady state of this microscopic device with or without the inner coupling using the Redfield master equation under a partial secular approximation. It is found that the functions as valve, refrigerator and amplifier in this quantum model can be realized in a large parametric space. And a valve-associated thermometer of low-temperature can be established without the assistance from the inner coupling of the system as well as the quantum coherence in the steady state. A high sensitivity of the indirect measurement of the low temperature of the sample can be obtained due to its nonlinear dependence on the temperatures of both the hot and the work terminals. Our study of such a multifunctional thermal device allows to provide a deeper insight to the underlying quantum thermodynamics mechanism associated with the quantum coherence, which is induced by the inner coupling and demonstrated in the steady state of the three-level system. Also, our model is a concise instance for integrating multiple thermal functions into a single microscopic system.

## I. INTRODUCTION

Classical thermodynamics based on the macroscopic statistics has been developed over two hundreds of years and has a mature theoretical framework. However it is always an interesting research project to incorporate quantum mechanics into thermodynamics, which stems from a microscopic theory about discrete levels and quantum coherence. Many literatures have made an active exploration about the role of quantumness in thermodynamics during the past two decades. These works on quantum thermodynamics can be roughly categorized into two divisions focused on the quantum effects from environment [1–4] and those from system [5–8], respectively. The present work is devoted to investigate the role of the steady-state coherence determined by the inner coupling of the system utilized as a multifunctional thermal device.

Various quantum thermodynamical functions, such as quantum valve [9–11], quantum refrigerator [12–14], quantum amplifier [15, 16], and quantum clock [17], have raised growing attentions in recent years. These models provide not only the fundamental physical platforms to test the macroscopic thermodynamic laws down to the level of quantum mechanics, but also the valuable references to design the microscopic quantum devices with certain thermal functions to actively and precisely tune the heat currents via the external macroscopic parameters, such as temperatures.

The measurement on the temperatures, especially on the low-temperatures of a microscopic system, is an open

problem in quantum thermodynamics. Precisely measuring the sample temperature in a very low region is particularly an important issue in the development of microscopic technologies. Thermometry at the microscopic scale has attracted a considerable amount of works in the fields of modern physics [18–21]. The smallest possible thermometer that composed merely of a single qubit was investigated in Ref. [22]. The authors studied the performance of the initial-state quantum coherence on the thermometer to discriminate a cold bath from a hot one. But it is necessary for that thermometer to find out the temperatures of both baths in advance. Thus the single-qubit thermometry determines whether a bath was hot or cold rather than obtains exactly the unknown temperature of the colder sample. Schemes of a true thermometer in both theoretical and experimental aspects have been proposed in a variety of experimental platforms. For examples, optical thermometers have been tested on the nitrogen-vacancy centres in diamond [19, 23] and quantum-dot system [24, 25]. Meanwhile, electronic thermometers have been available in the quantum-dot system [26–28] and in the superconducting qubits [29]. In particular, the low-temperature thermometry proposed in Ref. [29] is performed by a quantum Otto engine coupled to a hot reservoir with a known temperature  $T_h$  and a cold one with an unknown temperature  $T_c$ . A linear dependence of  $T_c$  on  $T_h$  was established when the heat engine is working with the Carnot efficiency. This result implies an instance to integrate multiple thermal functions into a single system.

We endeavor to study a multifunctional thermal device within the framework of the open-quantum-system theory. For a microscopic open system immersed in an environment, master equations allow to track the relevant degrees of freedom in both dynamics and steady-state

---

\* Email address: jingjun@zju.edu.cn

behavior, which are under the influence of all the other degrees of freedom that are not of the immediate interest or out of microscopic control [30–35]. Particularly, a perturbative expansion with respect to the system-bath coupling strength is employed to obtain a master equation for the system part. During an ordinary derivation, a Markovian approximation is first applied to obtain a Redfield master equation, and then a further secular approximation leads to the master equation in the well-known Lindblad form [30, 36]. The Redfield master equation retains the steady-state coherence of the system under a non-equilibrium environment [31–33], yet which may lose the positivity of the reduced density matrix in the short-time scale. In contrast, the Lindblad master equation [37, 38] always gives rise to a valid reduced density matrix upon the full secular approximation, yet fails to track the system coherence in the long-time limit. It was recently reported that the positivity of the Redfield master equation can be recovered by a partial secular approximation [39, 40].

In the present work, we investigate the steady-state quantum coherence induced by the inner-coupling within a microscopic model that is composed by a three-level system and three external thermal-baths with different temperatures. This model can be regarded as a thermal device with three terminals. Non-vanishing quantum coherence in the steady state is totally determined by the inner coupling of the system as demonstrated in the steady state. Certain thermal functions, such as valve, refrigerator and amplifier can be realized in this quantum model with the inner coupling. Based on the functions of valve and refrigerator, we further propose a quantum thermometer to measure the temperature of the coldest thermal bath. In particular, in the parametric space of the atomic-level spacings and the terminal temperatures, a sensitive thermometer can be realized at the working points of a quantum valve (also the onset of a quantum refrigerator).

The rest of this work is organized as following. In Sec. II, we present the total Hamiltonian of the model, including the interaction between the system and environments (the three thermal baths). Then we introduce the Redfield master equation with a partial secular approximation for this model with inner coupling. In Sec. III, it is demonstrated that the quantum coherence in the steady state is induced by the inner coupling. Certain multiple thermal functions are consequently realized, such as the valve and the amplifier for control the target heat current and the refrigerator to cool down the coldest bath. In Sec. IV, we present a theoretical scheme of a quantum thermometer for the coldest bath without the assistance from the inner-coupling of the system and also an accessible simulation proposal based on a double quantum-dot system. In Sec. V, we summarize the whole work.

## II. MODEL

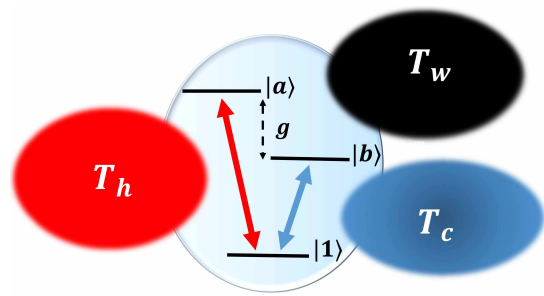


FIG. 1. Diagram of a three-level system coupled to three terminals. The three terminals can be regarded as three baths with different temperatures labelled as the hot ( $h$ ), cold ( $c$ ), and work ( $w$ ) bath, respectively.

In a typical thermodynamics model demonstrated in Fig. 1, a three-level microscopic system consisting of level-1,  $b$  and  $a$  by the increasing order of energy, is coupled to three terminals in their respective thermal equilibrium states. They are labelled respectively by  $h$ ,  $c$ , and  $w$  indicating their functions and temperatures. The total Hamiltonian for this model can be decomposed into the system Hamiltonian, the bath Hamiltonian and the interaction Hamiltonian:

$$H = H_S + H_B + H_{SB} \\ = H_S + \sum_{\mu=h,c,w} H_{\mu} + \sum_{\mu=h,c,w} S_{\mu} \otimes B_{\mu}. \quad (1)$$

In the system energy basis (also named the bare basis), the Hamiltonian can be written as ( $\hbar \equiv 1$ )

$$H_S = \sum_{l=a,b} \omega_l |l\rangle\langle l| + g(|a\rangle\langle b| + |b\rangle\langle a|), \quad (2)$$

where the ground energy has been set as  $\omega_1 = 0$  and  $g$  is the inner coupling strength between the two excited states [41]. The degenerate situation for  $\omega_a = \omega_b$  has been investigated in Ref. [5] about the application of a quantum refrigerator. It can be covered by our model. Each thermal bath is assumed to be a collection of decoupled harmonic oscillators with bosonic creation and annihilation operators  $b_{q,\mu}^{\dagger}$  and  $b_{q,\mu}$  for the mode  $q$  with frequency  $\omega_{q,\mu}$  in the bath  $\mu$ :

$$H_{\mu} = \sum_q \omega_{q,\mu} b_{q,\mu}^{\dagger} b_{q,\mu}. \quad (3)$$

The collective bath operators  $B_{\mu}$  in Eq. (1) describe the instantaneous displacement of bath oscillators from the equilibrium state,

$$B_{\mu} = \sum_q \lambda_{q,\mu} (b_{q,\mu}^{\dagger} + b_{q,\mu}). \quad (4)$$

The system operators  $S_\mu$  describe the interaction between the three-level system and the environments:

$$\begin{aligned} S_h &= |1\rangle\langle a| + |a\rangle\langle 1|, \\ S_c &= |1\rangle\langle b| + |b\rangle\langle 1|, \\ S_w &= (|a\rangle\langle a| - |b\rangle\langle b|) \sin \phi + (|a\rangle\langle b| + |b\rangle\langle a|) \cos \phi, \end{aligned} \quad (5)$$

where  $\phi \equiv \arctan(2g/\Delta)$  with  $\Delta \equiv \omega_a - \omega_b$ . The operator  $S_w$  depends explicitly on the inner coupling-strength  $g$  of the system. Energy current can be transferred among the hot, cold and work baths through the microscopic system.

### III. THREE-LEVEL SYSTEM WITH THE INNER COUPLING

The derivation onset of a microscopic master equation [36] for the open-quantum-system dynamics requires all the system operators to be expressed in eigenbasis  $|\lambda\rangle$  of the system Hamiltonian. In the present model, the Hamiltonian (2) of the three-level system with the inner coupling should be diagonalized as

$$\begin{aligned} H_S &= \sum_{\lambda=2,3} \omega_\lambda |\lambda\rangle\langle\lambda|, \\ \omega_{2,3} &= \frac{1}{2} \left( \omega_a + \omega_b \mp \sqrt{4g^2 + \Delta^2} \right), \\ |2\rangle &= \cos \frac{\phi}{2} |a\rangle - \sin \frac{\phi}{2} |b\rangle, \quad |3\rangle = \sin \frac{\phi}{2} |a\rangle + \cos \frac{\phi}{2} |b\rangle. \end{aligned}$$

Consequently, the coupling operators  $S_\mu$ ,  $\mu = h, c, w$ , in the interaction Hamiltonian  $H_{SB}$  are rewritten as

$$\begin{aligned} S_h &= \left( \cos \frac{\phi}{2} |1\rangle\langle 2| + \sin \frac{\phi}{2} |1\rangle\langle 3| \right) + h.c., \\ S_c &= \left( \cos \frac{\phi}{2} |1\rangle\langle 3| - \sin \frac{\phi}{2} |1\rangle\langle 2| \right) + h.c., \\ S_w &= |2\rangle\langle 3| + |3\rangle\langle 2|. \end{aligned} \quad (6)$$

The operators  $S_h$  and  $S_c$  in the eigenbasis indicate that the two excited states  $|3\rangle$  and  $|2\rangle$  are simultaneously coupled to the ground state  $|1\rangle$  via both the hot and the cold baths. These interaction channels as shown in Fig. 3 would induce quantum coherence in the density matrix spanned by  $\{|1\rangle, |2\rangle, |3\rangle\}$ . The bath- $w$  does work to the system through the operator  $S_w$ , which has been applied to the thermal rectification and the heat amplification [35].

#### A. Master equation and the steady state with quantum coherence

As derived in appendix A, the Redfield master equation with a partial secular approximation about the

present model can be explicitly expressed by

$$\begin{aligned} \dot{\rho}_S &= -i[H_S, \rho_S] + \sum_{\mu=h,c,w} \mathcal{D}_\mu[\rho_S], \\ \mathcal{D}_h[\rho_S] &= \Gamma_{h3}^+(\omega_3) \mathcal{L}_{\tau_{13}}(\rho_S) + \Gamma_{h3}^-(\omega_3) \mathcal{L}_{\tau_{31}}(\rho_S) \\ &+ \Gamma_{h2}^+(\omega_2) \mathcal{L}_{\tau_{12}}(\rho_S) + \Gamma_{h2}^-(\omega_2) \mathcal{L}_{\tau_{21}}(\rho_S) \\ &+ \sum_{m=2,3} \left\{ \Gamma_{h1}^-(\omega_m) [\tau_{m1} \rho_S \tau_{1\bar{m}} + \tau_{\bar{m}1} \rho_S \tau_{1m}] \right. \\ &\left. + \Gamma_{h1}^+(\omega_m) [\tau_{1m} \rho_S, \tau_{\bar{m}1}] + [\tau_{1\bar{m}}, \rho_S \tau_{m1}] \right\}, \\ \mathcal{D}_c[\rho_S] &= \Gamma_{c2}^+(\omega_3) \mathcal{L}_{\tau_{13}}(\rho_S) + \Gamma_{c2}^-(\omega_3) \mathcal{L}_{\tau_{31}}(\rho_S) \\ &+ \Gamma_{c3}^+(\omega_2) \mathcal{L}_{\tau_{12}}(\rho_S) + \Gamma_{c3}^-(\omega_2) \mathcal{L}_{\tau_{21}}(\rho_S) \\ &- \sum_{m=2,3} \left\{ \Gamma_{c1}^-(\omega_m) [\tau_{m1} \rho_S \tau_{1\bar{m}} + \tau_{\bar{m}1} \rho_S \tau_{1m}] \right. \\ &\left. + \Gamma_{c1}^+(\omega_m) ([\tau_{1m} \rho_S, \tau_{\bar{m}1}] + [\tau_{1\bar{m}}, \rho_S \tau_{m1}]) \right\}, \\ \mathcal{D}_w[\rho_S] &= \Gamma_w^+(\Omega) \mathcal{L}_{\tau_{23}}(\rho_S) + \Gamma_w^-(\Omega) \mathcal{L}_{\tau_{32}}(\rho_S), \end{aligned} \quad (7)$$

where the Lindblad superoperator is defined as  $\mathcal{L}_X(\rho_S) \equiv 2X\rho_S X^\dagger - X^\dagger X\rho_S - \rho_S X^\dagger X$ , with  $X$  an arbitrary system operator  $\tau_{nm} \equiv |n\rangle\langle m|$  ( $\bar{m} \equiv 5 - m$ ) and  $\Omega \equiv \omega_3 - \omega_2 = \sqrt{4g^2 + \Delta^2}$ . The transition rates can be factored as  $\Gamma_{\mu l}^\pm(\omega) = f_l \Gamma_\mu^\pm(\omega)$ ,  $l = 1, 2, 3$  and  $\mu = h, c, w$ , where  $f_1 = \sin \frac{\phi}{2} \cos \frac{\phi}{2}$ ,  $f_2 = \cos^2 \frac{\phi}{2}$ ,  $f_3 = \sin^2 \frac{\phi}{2}$ . And  $\Gamma_\mu^\pm(\omega)$  can be further factored as the product of  $G_\mu(\omega)$  and  $n_\mu(\mp\omega)$ , where  $G_\mu(\omega) \equiv 2\pi \sum_q |\lambda_{q,\mu}|^2 \delta(\omega_{q,\mu} - \omega)$  is the spectral density function of the bath- $\mu$  and  $n_\mu(\omega) = (e^{\beta_\mu \omega} - 1)^{-1}$  with  $\beta_\mu = 1/T_\mu$  ( $k_B \equiv 1$ ) is the average population determined by the temperature of bath- $\mu$ . In this work, the three baths are assumed to be Ohmic, i.e.,  $G_\mu(\omega) = \gamma_\mu \omega e^{-\omega/\omega_c}$ , where  $\gamma_\mu$  is a dimensionless system-bath coupling strength and  $\omega_c$  is the cutoff frequency characterizing the largest energy scale.

In comparison to the conventional Redfield master equation under the full secular approximation, there is an extra summation on the last two lines for both  $\mathcal{D}_h$  and  $\mathcal{D}_c$  in Eq. (7), which is the slowly-oscillating term retained by the partial secular approximation.

The master equation (7) yields a steady state  $\rho_{SS}$  in the following form:

$$\rho_{SS} = \begin{pmatrix} \rho_{11} & 0 & 0 \\ 0 & \rho_{22} & \rho_{23} \\ 0 & \rho_{32} & \rho_{33} \end{pmatrix}, \quad (8)$$

where the non-vanishing off-diagonal elements are obtained by letting  $\dot{\rho}_S = 0$  in Eq. (A11). In Fig. 2, the absolute value of coherence  $|\rho_{23}|$  measuring the quantumness of the three-level system demonstrates a nontrivial dependence on the inner coupling strength  $g$  and the temperature of the work bath  $T_w$ . A remarkable steady-state coherence  $|\rho_{23}|$  turns out with a moderate magnitude of  $g$  and roughly decreases with an increasing  $T_w$ . It is shown that a too small or a too big  $g$  and a high  $T_w$  are not

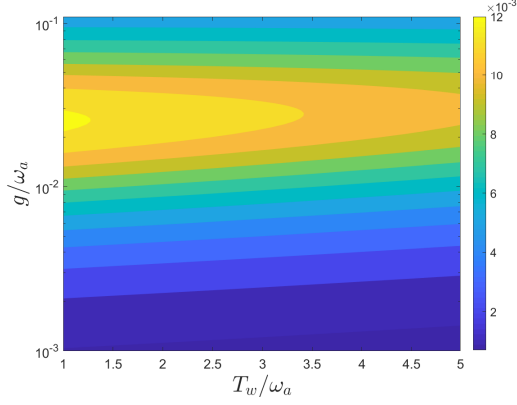


FIG. 2. The steady-state coherence  $|\rho_{23}|$  versus the inner coupling strength  $g$  and the temperature of the work bath  $T_w$ . The other parameters are  $\omega_b/\omega_a = 0.95$ ,  $\gamma_{h,c,w}/\omega_a = 0.008$ ,  $\omega_c/\omega_a = 50$ ,  $T_h/\omega_a = 1$  and  $T_c/\omega_a = 0.1$ .

favourable to the residue quantumness of the three-level system under the three thermal baths after a long-time evolution. The maximal value of  $|\rho_{23}|$  is achieved when  $g/\omega_a = 0.02$ , a weak inner-coupling strength that is numerically obtained under the parametric setting of Fig. 2.

### B. Thermal functions

A quantum system can be regarded as a microscopic thermal device when it can be used to control the heat currents back and forth from the system to the baths. In this subsection, it is shown that the open three-level system with inner coupling can be utilized as an integrated multifunctional thermal device with functions as valve, refrigerator and amplifier within certain parametric regions.

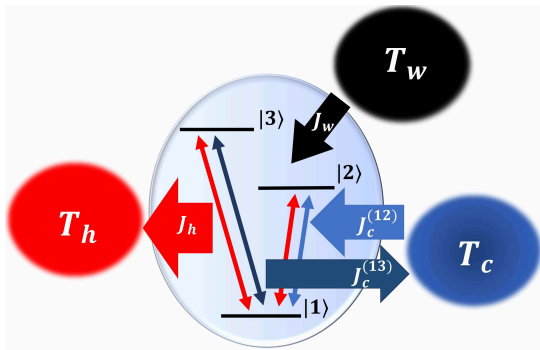


FIG. 3. Diagram of the heat currents  $J_\mu$  ( $\mu = h, c, w$ ) between the three-level system with inner coupling and the three thermal baths.  $J_c$  is described as the heat current between the three-level system and the cold bath, which is composed by  $J_c^{(12)}$  and  $J_c^{(13)}$  as displayed in Eq. (10).

The rate of the energy transfer between the system and the bath- $\mu$  ( $\mu = h, c, w$ ),  $\text{Tr}[H_S \mathcal{D}_\mu(\rho_S)]$ , defines the

corresponding heat current. In the long-time limit,  $\rho_S$  takes the steady-state solution  $\rho_{SS}$  given by Eq. (8). The standard formula for the (steady-state) rate of the heat exchange with bath- $\mu$  [5] is

$$J_\mu \equiv \text{Tr}[H_S \mathcal{D}_\mu(\rho_{SS})]. \quad (9)$$

Note a positive  $J_\mu$  means the heat current follows the direction from bath- $\mu$  to the central three-level system. By the master equation (7) and the definition about current in Eq. (9), the steady-state energy current between the three-level system and the cold bath can be decomposed into two parts, each in charge of the coupling between the energy-level pair  $\{|1\rangle, |l\rangle\}$  and the cold bath:

$$J_c = \sum_{l=2,3} J_c^{(1l)} = \sum_{l=2,3} 2\omega_l [\Gamma_{cl}^-(\omega_l)\rho_{11} - \Gamma_{cl}^+(\omega_l)\rho_{ll} + \Gamma_{c1}^+(\omega_l)(\rho_{23} + \rho_{32})], \quad (10)$$

where  $\bar{l} \equiv 5 - l$ . Similarly, the heat current between the three-level system and the hot bath can be expressed by

$$J_h = \sum_{l=2,3} 2\omega_l [\Gamma_{hl}^-(\omega_l)\rho_{11} - \Gamma_{hl}^+(\omega_l)\rho_{ll} - 2\Gamma_{h1}^+(\omega_l)(\rho_{23} + \rho_{32})]. \quad (11)$$

The steady-state quantum coherences, i.e., the terms  $\rho_{23}$  and  $\rho_{32}$ , contribute to both  $J_c$  and  $J_h$ . While the heat current between the three-level system and the work bath involves only with the populations on the two excited levels  $\{|2\rangle, |3\rangle\}$  of the system,

$$J_w = 2\Omega [\Gamma_w^-(\Omega)\rho_{22} - \Gamma_w^+(\Omega)\rho_{33}]. \quad (12)$$

These currents in Eqs. (10), (11) and (12) are drafted in Fig. 3. One can check that they follow the law of energy conservation (the first law of thermodynamics):  $J_c + J_h + J_w = 0$ . More detailed while cumbersome analytical expressions for the three currents can be directly obtained by the definitions of the decay rates  $\Gamma_{\mu,l}^\pm$  and the matrix elements  $\rho_{jk}$  of the steady state in Eq. (8). The following results about the steady-state currents under control are numerically obtained.

Here the work bath is used as a control terminal to manipulate the three currents embodying various thermal functions in the quantum regime. In analogy to a classical valve, a quantum thermal valve can precisely cut off the heat current from any one of the terminals while leaving the currents to flow through the other two terminals under special conditions. The three heat currents with respect to the temperature of control terminal  $T_w$  are demonstrated in Fig. 4(a), where the inner coupling strength  $g/\omega_a$  is set as 0.02. When  $T_w/\omega_a$  approaches a critical value, which is about 3.42 with the parameters we chosen in the plot, the energy current  $J_h$  vanishes while the other two currents do not. And then when  $T_w/\omega_a$  approaches another critical value (about 3.53), the heat current  $J_c$  disappears. These critical values are fully determined by the settings of the system energy structure



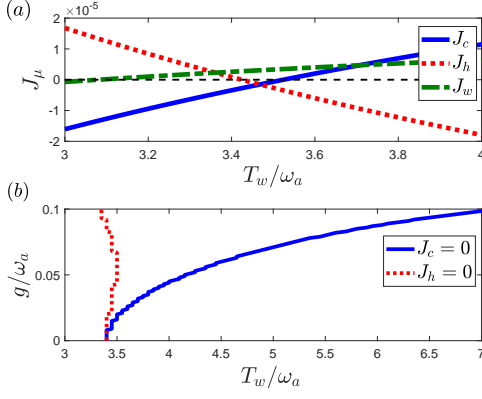


FIG. 4. The three-level system in the steady-state can be regarded as a valve for the current  $J_c$  or  $J_h$ . (a) The three heat currents  $J_\mu$  ( $\mu = c, h, w$ ) versus the temperature of work bath  $T_w$  with inner coupling strength  $g/\omega_a = 0.02$ . (b) The working spots ( $J_h = 0$  and  $J_c = 0$ ) of quantum valve by  $T_w$  and  $g$ . The other parameters are set as  $\omega_b/\omega_a = 0.8$ ,  $\gamma_{h,c,w}/\omega_a = 0.008$ ,  $\omega_c/\omega_a = 50$ ,  $T_h/\omega_a = 1$  and  $T_c/\omega_a = 0.85$ .

and the temperatures of the other two terminals. They are the working spots for the function as a quantum valve, which can be tuned by the inner coupling strength  $g$  as shown in Fig. 4(b). It is found that as long as  $T_w$  is over a critical value, the quantum thermal valve for  $J_c = 0$  can be realized by increasing  $g$ . A higher  $T_w$  corresponds to a larger  $g$ . In comparison, when  $T_w$  has been properly determined by the rest parameters, the choice of  $g$  for  $J_h = 0$  is almost irrelevant to the value of  $T_w$ .

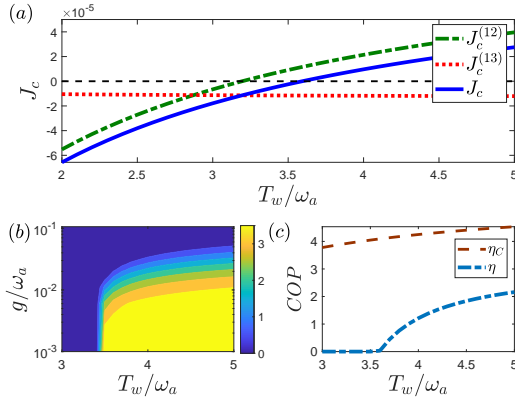


FIG. 5. The three-level system under the steady state can also be regarded as a refrigerator for the coldest bath. (a) The current  $J_c$  versus the temperature of work bath  $T_w$  with inner coupling strength  $g/\omega_a = 0.02$ . (b) The coefficient of cooling performance (COP) under various  $g$  and  $T_w$ . (c) COP versus  $T_w$  with  $g/\omega_a = 0.02$ . The other parameters are set as  $\omega_b/\omega_a = 0.8$ ,  $\gamma_{h,c,w}/\omega_a = 0.008$ ,  $\omega_c/\omega_a = 50$ ,  $T_h/\omega_a = 1$  and  $T_c/\omega_a = 0.85$ .

When focusing on the direction or signal of the current flows between the system and the cold bath, one can find that our three-level system under the steady state can be

used as a quantum refrigerator characterized by observing a net current flows out of the cold bath, i.e.  $J_c > 0$ . It means that by controlling the working terminal, the three-level system can continuously absorb the energy from the coldest terminal instead of importing energy to it. As shown in Fig. 5(a),  $J_c$  switches from negative to positive when  $T_w/\omega_a$  is over the critical point 3.53 of the quantum valve. According to Eq. (10),  $J_c$  can be decomposed of  $J_c^{(12)}$  and  $J_c^{(13)}$  (also shown in Fig. 3). The two sub-currents are the results by the coupling between respective energy-level pairs of the system and the cold bath. One can see that the heat current  $J_c^{(13)}$  stemming from the top level  $|3\rangle$  is always negative, i.e., the top level  $|3\rangle$  always conveys energy to the cold bath. It can be understood that the effective temperature for the energy-level pairs of  $\{|1\rangle, |3\rangle\}$  is always higher than the temperature of bath- $c$ . That is supported by the existence of inner coupling within the three-level system. In contrast,  $J_c^{(12)}$  could become positive by increasing  $T_w$ . In the refrigerator regime depending on the working bath,  $J_c > 0$  and  $J_w > 0$ . According to the first law of thermodynamics, the heat current  $J_h$  follows the direction from the central three-level system to the bath- $h$ , i.e.,  $J_h < 0$ . Figure 3 describes all the directions of the heat currents between the refrigerator system and the three thermal baths.

The coefficient of cooling performance (COP) in the cooling regime, i.e.,  $J_c > 0$ , which is defined as  $\eta \equiv J_c/J_w$  [5], presents in Fig. 5(b). It is shown that the cooling efficiency of our quantum refrigerator will be gradually degraded with an increasing inner-coupling. In Fig. 5(c), we also compare the COP of our refrigerator with the Carnot limit  $\eta_C$ :

$$\eta_C \equiv \frac{\beta_h - \beta_w}{\beta_c - \beta_h}, \quad (13)$$

which is the upper bound of the cooling efficiency for the thermal-machine. Meanwhile, due to the Clausius theorem for the second law of thermodynamics, we have

$$\frac{\dot{Q}_c}{T_c} + \frac{\dot{Q}_h}{T_h} + \frac{\dot{Q}_w}{T_w} = \frac{J_c}{T_c} + \frac{J_h}{T_h} + \frac{J_w}{T_w} \leq 0, \quad (14)$$

where  $\dot{Q}_\mu$ ,  $\mu = h, c, w$ , is the heat current transferred between the system and bath- $\mu$ . Based on the first and second laws of thermodynamics, one can obtain

$$\eta \equiv \frac{J_c}{J_w} \leq \frac{T_h - T_w}{T_c - T_h} \cdot \frac{T_c}{T_w} = \frac{\beta_h - \beta_w}{\beta_c - \beta_h} = \eta_C. \quad (15)$$

It is shown in Fig. 5(c) that  $\eta$  is always less than  $\eta_C$ .

An overall picture for the thermal functions of valve and refrigerator can be illustrated by a phase diagram in Fig. 6 for the heat current  $J_c$  with the temperature of the work bath  $T_w$  and the inner coupling  $g$ . The red belt consisting of the working spots with  $J_c = 0$  for the quantum valve of the heat current between the system and the cold bath separates the refrigerator regime (the

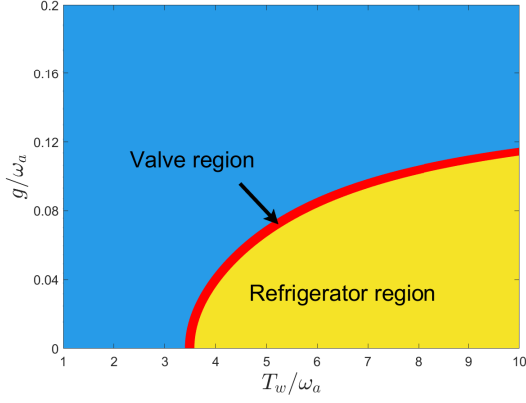


FIG. 6. The phase diagram of the thermal functions of valve and refrigerator in the parametric space of the temperature of the work bath  $T_w$  and the inner coupling strength  $g$ . The other parameters are set as  $\omega_b/\omega_a = 0.8$ ,  $\gamma_{h,c,w}/\omega_a = 0.008$ ,  $\omega_c/\omega_a = 50$ ,  $T_h/\omega_a = 1$  and  $T_c/\omega_a = 0.85$ .

yellow region) with  $J_c > 0$  from the remain parametric regime. One can roughly observe that a strong inner coupling accompanied by a high-temperature work bath is useful to realize quantum valve and refrigerator.

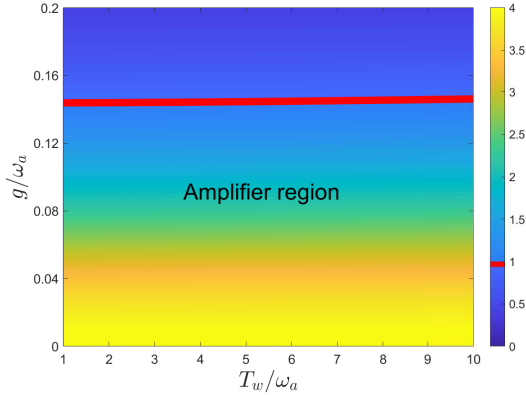


FIG. 7. The amplification factor  $\alpha_J$  under various temperatures of the work bath  $T_w$  and the inner coupling strength  $g$ . The other parameters are set as  $\omega_b/\omega_a = 0.8$ ,  $\gamma_{h,c,w}/\omega_a = 0.008$ ,  $\omega_c/\omega_a = 50$ ,  $T_h/\omega_a = 1$  and  $T_c/\omega_a = 0.85$ .

In the same parametric space as in Fig. 6, we can also show the region of a quantum thermal amplifier set up by our model. Here we focus on the variation of the heat current between the work bath and the system  $J_w$  upon that of the current between the cold bath and the system  $J_c$ , i.e., the amplification factor [15]  $\alpha_J \equiv |\partial J_c / \partial J_w|$ . Due to this definition, an amplifier can be realized when  $\alpha_J > 1$ . A larger amplification factor means a stronger amplification capacity about the working current  $J_w$ . The region of the amplification factor  $\alpha_J > 1$  is distinguished in Fig. 7, where the red line implies the boundary between amplification and contraction  $\alpha_J < 1$ . It is clear that the three-level microscopic system with a small inner-

coupling can be utilized as an amplifier. By observing the overlap between the region of valve and refrigerator in Fig. 6 and that of the amplifier in Fig. 7, one can find that all of these thermal functions can be realized in our model with a finite inner-coupling strength  $g$  under the same parametric setting.

#### IV. THREE-LEVEL SYSTEM WITHOUT THE INNER COUPLING

In this section, we assume a vanishing inner-coupling strength within the system, i.e.,  $g = 0$ . In this condition, the system Hamiltonian is diagonal in the bare basis  $\{|1\rangle, |a\rangle, |b\rangle\}$ . The coupling operators  $S_h$  and  $S_c$  are the same as those in Eq. (5), and the operator  $S_w$  reduces to

$$S_w = |a\rangle\langle b| + |b\rangle\langle a|. \quad (16)$$

Now the interaction with the work bath merely induces the energy exchange between the two excited states without affecting their energy levels.

##### A. The steady state without quantum coherence

The absence of the inner-coupling  $g = 0$  renders  $\phi = 0$ . Thus the master equation (7) reduces to

$$\dot{\rho}_S = -i[H_S, \rho_S] + \sum_{\mu=h,c,w} \mathcal{D}_\mu[\rho_S], \quad (17)$$

$$\begin{aligned} \mathcal{D}_h[\rho_S] &= \Gamma_h^+(\omega_a) \mathcal{L}_{\tau_{1a}}(\rho_S) + \Gamma_h^-(\omega_a) \mathcal{L}_{\tau_{a1}}(\rho_S), \\ \mathcal{D}_c[\rho_S] &= \Gamma_c^+(\omega_b) \mathcal{L}_{\tau_{1b}}(\rho_S) + \Gamma_c^-(\omega_b) \mathcal{L}_{\tau_{b1}}(\rho_S), \\ \mathcal{D}_w[\rho_S] &= \Gamma_w^+(\Delta) \mathcal{L}_{\tau_{ba}}(\rho_S) + \Gamma_w^-(\Delta) \mathcal{L}_{\tau_{ab}}(\rho_S). \end{aligned}$$

In the long-time limit, the master equation (17) gives rise to a diagonal steady-state of the system:

$$\rho_{SS} = \begin{pmatrix} \rho_{11} & 0 & 0 \\ 0 & \rho_{bb} & 0 \\ 0 & 0 & \rho_{aa} \end{pmatrix}, \quad (18)$$

where

$$\begin{aligned} \rho_{11} &= \frac{\Gamma_c^+(\omega_b)[\Gamma_h^+(\omega_a) + \Gamma_w^+(\Delta)] + \Gamma_h^+(\omega_a)\Gamma_w^-(\Delta)}{\Lambda}, \\ \rho_{bb} &= \frac{\Gamma_c^-(\omega_b)[\Gamma_h^+(\omega_a) + \Gamma_w^+(\Delta)] + \Gamma_h^-(\omega_a)\Gamma_w^+(\Delta)}{\Lambda}, \\ \rho_{aa} &= \frac{\Gamma_h^-(\omega_a)[\Gamma_c^+(\omega_b) + \Gamma_w^-(\Delta)] + \Gamma_c^-(\omega_b)\Gamma_w^-(\Delta)}{\Lambda}, \end{aligned} \quad (19)$$

with the normalization factor  $\Lambda = \Gamma_h^+(\omega_a)\Gamma_c^+(\omega_b) + \Gamma_c^+(\omega_b)\Gamma_w^+(\Delta) + \Gamma_h^+(\omega_a)\Gamma_w^-(\Delta) + \Gamma_h^-(\omega_a)\Gamma_c^-(\omega_b) + \Gamma_c^-(\omega_b)\Gamma_w^-(\Delta) + \Gamma_h^-(\omega_a)\Gamma_w^+(\Delta) + \Gamma_h^-(\omega_a)\Gamma_c^+(\omega_b) + \Gamma_c^-(\omega_b)\Gamma_w^+(\Delta) + \Gamma_h^-(\omega_a)\Gamma_w^-(\Delta)$ . Physically, the three quantum channels connecting the thermal baths and the system are separable in the absence of the inner-coupling. The dynamics of the populations and coherence in this

model are therefore naturally decoupled from each other. Consequently the quantum coherence vanishes in the long-time limit.

The steady-state solution certainly satisfies the principle of detailed balance. Note the rates of  $\Gamma_\mu^+(\omega)$  and  $\Gamma_\mu^-(\omega)$  represent the probabilities of the decay and excitation transitions, respectively. Due to the conservation of the total population in the steady state, the probabilities of the population gain must be equivalent to the population loss for each level. In particular, we have

$$\begin{aligned}\Gamma_c^+(\omega_b)\rho_{bb} + \Gamma_h^+(\omega_a)\rho_{aa} &= [\Gamma_c^-(\omega_b) + \Gamma_h^-(\omega_a)]\rho_{11}, \\ \Gamma_c^-(\omega_b)\rho_{11} + \Gamma_w^+(\Delta)\rho_{aa} &= [\Gamma_w^-(\Delta) + \Gamma_c^+(\omega_b)]\rho_{bb}, \\ \Gamma_h^-(\omega_a)\rho_{11} + \Gamma_w^-(\Delta)\rho_{bb} &= [\Gamma_h^+(\omega_a) + \Gamma_w^+(\Delta)]\rho_{aa}.\end{aligned}\quad (20)$$

The result in Eq. (19) can be determined by the solution of Eq. (20) and the normalization condition without invoking the master equation.

### B. Microscopic Thermometer

While temperature is an intuitive notion deeply rooted in the daily life as well as the classical world, yet it is subtle and surprisingly difficult to formalise in quantum mechanics, especially in the field of low temperature region [18, 42]. In this subsection, we introduce a quantum thermometer to estimate the temperature of the coldest bath in the model of a three-level system without inner-coupling. Here baths- $c$ ,  $h$ , and  $w$  are respectively labelled as the sample, conductor, and control terminals in literatures and it is assumed that the sample temperature cannot be directly measured, in contrast to the temperatures of the conductor and the control terminals.

Due to the definition in Eq. (9), the steady-state energy current between the sample and the system is given by

$$J_c = 2\omega_b[\Gamma_c^-(\omega_b)\rho_{11} - \Gamma_c^+(\omega_b)\rho_{bb}]. \quad (21)$$

In comparison with Eq. (10),  $J_c$  is now equivalent to  $J_c^{(12)}$  having no contribution from quantum coherence. Similarly, the heat currents between the conductor and control terminals and the system are respectively given by

$$J_h = 2\omega_a[\Gamma_h^-(\omega_a)\rho_{11} - \Gamma_h^+(\omega_a)\rho_{aa}], \quad (22)$$

$$J_w = 2\Delta[\Gamma_w^-(\Delta)\rho_{bb} - \Gamma_w^+(\Delta)\rho_{aa}]. \quad (23)$$

In Figs. 8(a) and (b), the heat currents are described by Eqs. (21), (22), and (23) with respect to the temperature of the control terminal  $T_w$ . It is shown that our three-level system in the absence of the inner coupling can work as a special thermal valve for both  $J_c$  and  $J_h$  when  $J_w$  is switched off. The particular working points of the valve depend on the choice about the other parameters. The parameters including the temperatures of the three baths would determine the population distributions on the three levels of our system. One can then define two effective temperatures for the energy-level pairs of

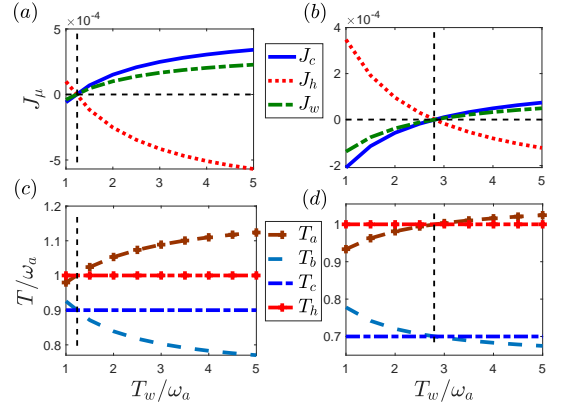


FIG. 8. The thermal behaviors vary with temperature of the control terminal in the model without the inner coupling. (a) and (b): the heat currents towards the three terminals with  $T_c/\omega_a = 0.9$  and  $T_c/\omega_a = 0.7$ , respectively. (c) and (d): the effective temperatures under the same conditions about  $T_c$  for (a) and (b), respectively. The other parameters are set as  $\omega_b/\omega_a = 0.6$ ,  $T_h/\omega_a = 1$ ,  $\gamma_{c,h,w}/\omega_a = 0.008$  and  $\omega_c/\omega_a = 50$ .

$\{|1\rangle, |a\rangle\}$  and  $\{|1\rangle, |b\rangle\}$  due to the Boltzmann distribution. They read,

$$T_s = \omega_s / \ln \left( \frac{\rho_{ss}}{\rho_{11}} \right), \quad s = a, b. \quad (24)$$

In general situations for the non-equilibrium steady state, the nonzero currents  $J_c$  and  $J_h$  will lead to  $T_h \neq T_a$  and  $T_c \neq T_b$  as demonstrated in Figs. 8(c) and 8(d). Thus at the working points of quantum valve, for instances  $T_w/\omega_a = 1.2$  under  $T_h/\omega_a = 1$ ,  $T_c/\omega_a = 0.9$  in Fig. 8(c) and  $T_w/\omega_a = 2.8$  under  $T_h/\omega_a = 1$ ,  $T_c/\omega_a = 0.7$  in Fig. 8(d), all the heat currents vanish and the quantum system reaches a thermal equilibrium state. It thus guarantees  $T_a = T_h$  and  $T_b = T_c$  and the self-consistency about the effective temperatures. In another word, the populations of the three-level system in the thermal equilibrium state [see the two instances in Figs. 8(c) and 8(d)] satisfy

$$\frac{\rho_{aa}}{\rho_{11}} = e^{-\frac{\omega_a}{T_h}}, \quad \frac{\rho_{aa}}{\rho_{bb}} = e^{-\frac{\Delta}{T_w}}, \quad \frac{\rho_{bb}}{\rho_{11}} = e^{-\frac{\omega_b}{T_c}}. \quad (25)$$

These expressions yield

$$\frac{\omega_a}{T_h} = \frac{\Delta}{T_w} + \frac{\omega_b}{T_c}. \quad (26)$$

Note again that the two  $T_w$ 's in Fig. 8 are two special cases in accordance to the choices of bath-temperatures, system energy configuration, and the interaction strengthes with the baths. In particular, a proper  $T_w$  for an equilibrium state can always be obtained by sweeping over the parametric space when  $T_c$  is settled and it increases with a decreasing  $T_c$ . Efficient cooling a lower temperature sample requires more energy input from the control terminal with a higher temperature.

The three-level system under the thermal equilibrium state can be used to switch on the quantum functions of both valve and refrigerator. In particular, the working points ( $J_c = 0$ ) for the quantum valve are the onset point for the quantum refrigerator ( $J_c > 0$ ). The coefficient of cooling performance of our system without the inner coupling is

$$\eta \equiv \frac{J_c}{J_w} = \frac{\omega_b}{\Delta}, \quad (27)$$

which is obtained by Eqs. (20), (21) and (23). Comparing to the  $T_w$ -dependent result (see Fig. 5) in the nonvanishing inner-coupling situation, now the COP  $\eta$  becomes a constant  $\omega_b/\Delta = \omega_b/(\omega_a - \omega_b)$ . Taking Eq. (26) into account, it is interesting to find that the equivalence in Eq. (15), i.e., the Carnot limit, can be achieved at the working points of the quantum valve. With respect to the quantum refrigerator, according to Eq. (21),  $J_c \geq 0$  means

$$\Gamma_c^-(\omega_b)\Gamma_h^+(\omega_a)\Gamma_w^-(\Delta) \geq \Gamma_c^+(\omega_b)\Gamma_h^-(\omega_a)\Gamma_w^+(\Delta), \quad (28)$$

where  $\Gamma_\mu^\pm(\omega) = G_\mu(\omega)n_\mu(\mp\omega)$  with  $G_\mu(\omega)$  the spectral density function and  $n_\mu(\omega)$  the average occupation number of bath- $\mu$ . Immediately we have

$$e^{\beta_h\omega_a} \geq e^{\beta_c\omega_b}e^{\beta_w\Delta}, \quad (29)$$

which is equivalent to Eq. (15). Thus the onset of the cooling windows as well as the refrigerator performance of our multifunctional device in the absence of the inner coupling is always consistent with the Carnot limit.

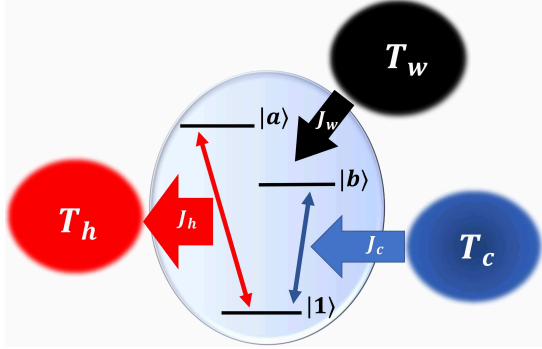


FIG. 9. Diagram of the directions of heat currents  $J_\mu$  ( $\mu = h, c, w$ ) between the system without the inner coupling and the three thermal terminals in the refrigerator regime.

In the refrigerator regime,  $J_c > 0$  means  $J_w > 0$  and  $J_h < 0$ . Their directions are shown in Fig. 9. One can therefore observe the heat current flows from the sample to the conductor through the three-level system. According to the definitions of the effective temperatures in Eq. (24), the effective temperatures of the system and the temperatures of terminal- $h$  and - $c$  can be ordered by  $T_b < T_c < T_h < T_a$ .

More importantly, the sample temperature  $T_c$  can be immediately obtained as

$$T_c = \frac{T_h T_w \xi}{T_w - (1 - \xi)T_h}, \quad (30)$$

where  $\xi \equiv \omega_b/\omega_a$ , by the thermal equilibrium condition. This relation between  $T_c$  and the other two temperatures indicates an indirect measurement approach for  $T_c$  by measuring the control temperature  $T_w$  when the system moves into a thermal-equilibrium state. In addition, the energy-configuration parameter of the three-level system  $\xi$  and the temperature of conductor terminal  $T_h$  are supposed to be determined in advance.

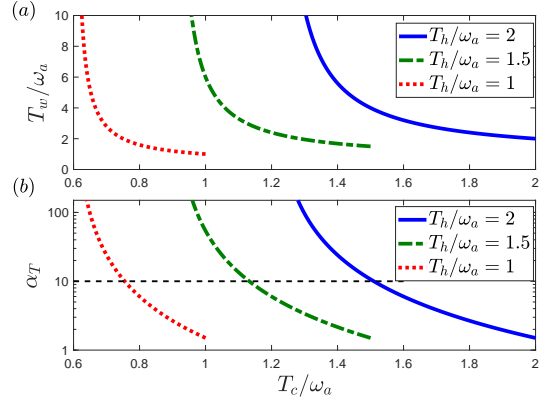


FIG. 10. Under different conductor temperature  $T_h$ , (a) the control temperature  $T_w$  as a function of the sample temperature  $T_c$ ; (b) the measurement sensitivity for the quantum thermometer  $\alpha_T$  as a function of  $T_c$ . The energy-configuration parameter is set as  $\xi = 0.6$ .

From Eq. (30), the lower bound of the sample temperature that can be measured by our thermometer is determined by

$$\lim_{T_w \rightarrow \infty} T_c = \xi T_h = \frac{\omega_b}{\omega_a} T_h, \quad (31)$$

which means that the measurement range for  $T_c$  is linearly proportional to both  $T_h$  and the energy-configuration parameter  $\xi$ . This result under an infinite high-temperature control terminal coincides with that obtained by a previous proposal about the quantum thermometer connecting to a quantum thermal machine [29], in which the sample temperature  $T_c$  has a linear relationship with the conduct terminal  $T_h$ . In the present thermometer scheme, however, we have a non-linear relation between the sample temperature and the control temperature:

$$\frac{T_c}{T_w} = \frac{\xi}{\xi - 1} + \frac{\xi}{(\xi - 1)^2} \frac{T_w}{T_h} + \frac{\xi}{(\xi - 1)^3} \left( \frac{T_w^2}{T_h^2} \right) + \mathcal{O} \left( \frac{T_w^3}{T_h^3} \right). \quad (32)$$

Thus our proposal might provide a more sensitive measurement on  $T_c$  than the existing one.



In Fig. 10(a), we display the dependence of the control temperature  $T_w$  on the sample temperature  $T_c$  under three different conductor temperatures  $T_h$  and a fixed parameter  $\xi = 0.6$ . Note  $T_c \leq T_h$  according to the definition and  $T_c \geq \xi T_h$  due to the constraint by Eq. (31). As also shown in Fig. 10(a), the variation of  $T_w$  with respect to  $T_c$  is rapidly enhanced by decreasing  $T_c$ . This behavior is more clear in the measurement sensitivity [18]  $\alpha_T$  shown in Fig. 10(b), which is defined as the absolute value of the control temperature bias divided by the sample-temperature variation:

$$\alpha_T \equiv \left| \frac{\partial T_w}{\partial T_c} \right| = \frac{\xi(1-\xi)T_h^2}{(\xi T_h - T_c)^2}. \quad (33)$$

Then for a prescribed critical value of the sensitivity  $\alpha_T$ , a high-precision measurement region for the sample temperature can be confirmed as  $(\xi T_h, T'_c]$ , where the so-called critical sample temperature  $T'_c$  is

$$T'_c = \xi T_h + \sqrt{\frac{\xi(1-\xi)T_h^2}{\alpha_T}}. \quad (34)$$

In Fig. 10(b), we set  $\alpha_T = 10$  as displayed by the horizontal dashed line. Then the cross points of the vertical lines and the horizontal line are critical temperatures  $T'_c(\alpha_T)$ . For example, when  $T_h/\omega_a = 2$  and  $\xi = 0.6$ , one can perform a high-precision indirect measurement for the sample temperatures in the range  $1.2 < T_c/\omega_a \leq 1.51$  with at least one-order amplification in the magnitude of the temperature variation.

### C. Experimental simulation of the microscopic low-temperature thermometer

The quantum-dot systems as a kind of experimental platform have been widely applied in the field of quantum thermodynamics to simulate or realize various thermal functions, such as the heat engine [43–45], the refrigerator [46–50], the novel energy carrier [26, 51, 52], and a Maxwell demon in the strong-coupling regime [53]. Here we can show that a quantum-dot system can also be used to display the thermometer function in the proceeding subsection, by simulating the heat currents with the charge currents.

A three-terminal quantum-dot thermometer is considered in Fig. 11. The three-level system can be mimicked by a double-quantum-dot system which consists of two capacitively coupled quantum dots (QD<sub>1</sub> and QD<sub>2</sub>) operated in the Coulomb-blockade regime. The system is coupled to three terminals characterized by the two metal leads and a radiation field, which are labelled respectively by  $h$ ,  $c$ , and  $w$  [43]. The temperatures of the three terminals satisfy the same ordering set up by our theoretical proposal:  $T_c < T_h < T_w$ . The terminal- $h(c)$  can only exchange electrons with the QD<sub>1(2)</sub>. The corresponding

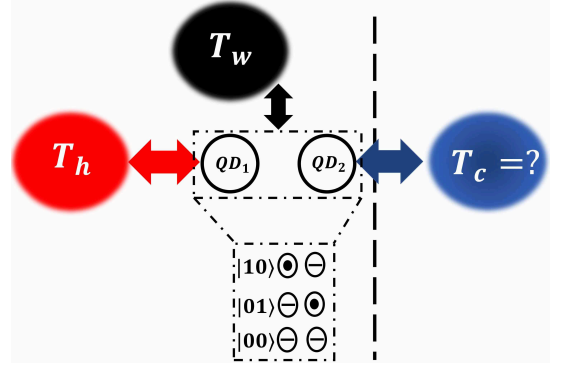


FIG. 11. An experimental scheme for the quantum thermometer established in our microscopic device, which can be realized by an open double-quantum-dot system having a single electron coupled to three independent baths consisting of two metal leads and a radiation field. The three levels  $|1\rangle$ ,  $|b\rangle$ , and  $|a\rangle$  of the central system in our theoretical model (see Fig. 9) can be mapped to the electron states  $|00\rangle$ ,  $|01\rangle$ , and  $|10\rangle$ , respectively.

Hamiltonian [43] is

$$H = H_0 + V_M + V_P, \quad (35)$$

$$H_0 = \sum_{m=1,2} \varepsilon_m c_m^\dagger c_m + \sum_{\mu=h,c} \varepsilon_\mu b_\mu^\dagger b_\mu + \sum_\alpha \omega_\alpha a_\alpha^\dagger a_\alpha \quad (36)$$

$$V_M = (V_{1h} c_1 b_h^\dagger + V_{2c} c_2 b_c^\dagger) + \text{H.c.}, \quad (37)$$

$$V_P = \sum_\alpha (V_\alpha a_\alpha c_2^\dagger c_1 + \text{H.c.}). \quad (38)$$

The three terms in the free Hamiltonian  $H_0$  of Eq. (36) describe the isolated quantum dots, the free leads, and the radiation field, respectively.  $c$  ( $c^\dagger$ ),  $b$  ( $b^\dagger$ ) and  $a$  ( $a^\dagger$ ) are the annihilation (creation) operators for the electron in QD, the electron along the lead, and the photons, respectively. The Hamiltonian  $V_M$  in Eq. (37) describes the coupling between the quantum dots and the metal leads. The Hamiltonian  $V_P$  in Eq. (38) describes the dot-radiation-field interaction, addressing both the driving and the spontaneous light emission. Similar Hamiltonians can also be found in Refs. [54, 55].

A remarkable feature of the Coulomb-coupled quantum-dot system is that the electron transport through the system is forbidden but the capacitive coupling between the two dots allows electronic fluctuations to transmit heat between the terminals [26, 56]. Coulomb interactions prevent two electrons from being present at the same time in the Coulomb-blockade regime. The Coulomb-coupled quantum-dot system in the subspace spanned by  $\{|00\rangle, |01\rangle, |10\rangle\}$  constitutes an artificial three-level atom [26, 43, 47], where the energy levels  $|1\rangle$  and  $|0\rangle$  indicate the state of the quantum dot occupied by one and zero electron, respectively. Then the three states of the center system in our model could be mapped to the double-dot system in the single-electron subspace by  $|1\rangle \leftrightarrow |00\rangle$ ,  $|a\rangle \leftrightarrow |10\rangle$  and  $|b\rangle \leftrightarrow |01\rangle$ . The different dot energies  $\varepsilon_1$  and  $\varepsilon_2$  can be regarded as the

energy gaps  $\omega_a$  and  $\omega_b$ , respectively. The energy configuration of the quantum-dot system [ $\xi$  in Eq. (30)] can be determined by manipulating the gate voltage in advance [46].

The thermometer by the quantum-dot system can be implemented by the following procedure. As indicated by Fig. 8, one can start from  $T_w = T_h$ , and increase  $T_w$  until  $J_h = 0$ , which is in experiment the charge current between the central system and the conductor terminal. At this working-point, the quantum-dot system actually reaches a thermal equilibrium state. Then the temperature of sample terminal  $T_c$  can be obtained by measuring  $T_w$  according to Eq. (30).

## V. CONCLUSION

In conclusion, we have investigated the steady-state thermal functions realized in an open-quantum-system model of a three-level system attached to three thermal baths with or without inner coupling. The residue quantum coherence in steady-state is obtained by the Redfield master equation with a partial secular approximation. It is found that a microscopic multifunctional thermal device can be established by varying the inner coupling within the system and the temperatures of the external baths. We identify the respective working regimes for the thermal functions as valve, refrigerator, and amplifier.

We also demonstrate that the three-level system can be utilized as a microscopic thermometer to determine the temperature of coldest terminal in the absence of the inner coupling. The quantum thermometer is established when the three-level system reaches the thermal equilibrium state under the three terminals, which also switches on the functions of valve and refrigerator. We find a non-linear dependence of the sample-temperature on the hot and the control temperatures, which could be exploited to perform a high-precision measurement. Our work provides a deep insight to understand the roles of the system quantumness and the inner-coupling in quantum thermodynamics.

## ACKNOWLEDGEMENTS

We acknowledge grant support from the National Science Foundation of China (Grants No. 11974311 and No. U1801661), Zhejiang Provincial Natural Science Foundation of China under Grant No. LD18A040001, and the Fundamental Research Funds for the Central Universities (No. 2018QNA3004).

### Appendix A: The master equation under the partial secular approximation

In this appendix, we derive the master equation (7) in the main text under the partial secular approximation.

It is of a Redfield master equation that conserves the positivity of the reduced density matrix even in the short-time scale.

The interaction Hamiltonian describing the coupling between the three-level system and the three thermal baths in Eq. (1) can be written as

$$H_{SB} = \sum_{\mu=h,c,w} H_{SB}^{\mu} = \sum_{\mu=h,c,w} S_{\mu} \otimes B_{\mu}. \quad (\text{A1})$$

In the interaction picture with respect to  $H_S + H_B$ , it becomes

$$H_{SB}(t) = \sum_{\mu=h,c,w} H_{SB}^{\mu}(t) = \sum_{\mu=h,c,w} S_{\mu}(t) \otimes B_{\mu}(t), \quad (\text{A2})$$

where

$$S_h(t) = \cos \frac{\phi}{2} (\tau_{12} e^{-i\omega_2 t} + \tau_{21} e^{i\omega_2 t}) + \sin \frac{\phi}{2} (\tau_{13} e^{-i\omega_3 t} + \tau_{31} e^{i\omega_3 t}), \quad (\text{A3})$$

$$S_c(t) = \cos \frac{\phi}{2} (\tau_{13} e^{-i\omega_3 t} + \tau_{31} e^{i\omega_3 t}) - \sin \frac{\phi}{2} (\tau_{12} e^{-i\omega_2 t} + \tau_{21} e^{i\omega_2 t}), \quad (\text{A4})$$

$$S_w(t) = \tau_{23} e^{-i\Omega t} + \tau_{32} e^{i\Omega t}, \quad (\text{A5})$$

with  $\tau_{mn} \equiv |m\rangle\langle n|$  and  $\Omega \equiv \omega_3 - \omega_2$ . The collective bath operators are

$$B_{\mu}(t) = \sum_q \lambda_{q,\mu} (b_{q,\mu} e^{-i\omega_{q,\mu} t} + b_{q,\mu}^{\dagger} e^{i\omega_{q,\mu} t}). \quad (\text{A6})$$

Under the assumptions of a weak coupling between the microscopic system and the thermal baths (Born-approximation) and an ignorable relaxation time-scale for the thermal baths (Markovian approximation), one can apply the Redfield master equation to investigate the central-system dynamics to the second order of the coupling strength:

$$\dot{\rho}_S = - \int_0^{\infty} ds \text{Tr}_B [H_{SB}(t), [H_{SB}(t-s), \rho_S \otimes \rho_B]]. \quad (\text{A7})$$

The commutator operators in Eq. (A7) expands as

$$\begin{aligned} & [H_{SB}(t), [H_{SB}(t-s), \rho_S \otimes \rho_B]] \\ &= H_{SB}(t) H_{SB}(t-s) \rho_S \rho_B - H_{SB}(t) \rho_S \rho_B H_{SB}(t-s) \\ & - H_{SB}(t-s) \rho_S \rho_B H_{SB}(t) + \rho_S \rho_B H_{SB}(t-s) H_{SB}(t). \end{aligned} \quad (\text{A8})$$

Partial tracing over the degrees of freedom of the baths upon substituting the interaction Hamiltonian (A2) into the master equation (A7) turns out to be a summation over 12 terms. The derivation is tedious but straightforward.

ward. A typical term presents as following:

$$\begin{aligned}
& \text{Tr}_B [H_{SB}^h(t) \rho_S \rho_B H_{SB}^h(t-s)] \\
&= \Gamma_{h3}^+(\omega_3) [\tau_{13} \rho_S \tau_{13} e^{-2i\omega_3 t} + \tau_{13} \rho_S \tau_{31}] \\
&+ \Gamma_{h1}^+(\omega_3) [\tau_{13} \rho_S \tau_{12} e^{-i(\omega_2+\omega_3)t} + \tau_{13} \rho_S \tau_{21} e^{-i(\omega_3-\omega_2)t}] \\
&+ \Gamma_{h3}^-(\omega_3) [\tau_{31} \rho_S \tau_{13} + \tau_{31} \rho_S \tau_{31} e^{2i\omega_3 t}] \\
&+ \Gamma_{h1}^-(\omega_3) [\tau_{31} \rho_S \tau_{12} e^{i(\omega_3-\omega_2)t} + \tau_{31} \rho_S \tau_{21} e^{i(\omega_3+\omega_2)t}] \\
&+ \Gamma_{h2}^+(\omega_2) [\tau_{12} \rho_S \tau_{12} e^{-2i\omega_2 t} + \tau_{12} \rho_S \tau_{21}] \\
&+ \Gamma_{h1}^+(\omega_2) [\tau_{12} \rho_S \tau_{13} e^{-i(\omega_2+\omega_3)t} + \tau_{12} \rho_S \tau_{31} e^{-i(\omega_2-\omega_3)t}] \\
&+ \Gamma_{h2}^-(\omega_2) [\tau_{21} \rho_S \tau_{12} + \tau_{21} \rho_S \tau_{21} e^{2i\omega_2 t}] \\
&+ \Gamma_{h1}^-(\omega_2) [\tau_{21} \rho_S \tau_{13} e^{i(\omega_2-\omega_3)t} + \tau_{21} \rho_S \tau_{31} e^{i(\omega_2+\omega_3)t}].
\end{aligned} \tag{A9}$$

Here the decay rates are defined as  $\Gamma_{hl}^\pm(\omega) = \Gamma_h^\pm(\omega) f_l$  with the factors  $f_1 = \sin \frac{\phi}{2} \cos \frac{\phi}{2}$ ,  $f_2 = \cos^2 \frac{\phi}{2}$ ,  $f_3 = \sin^2 \frac{\phi}{2}$  and  $\Gamma_h^\pm(\omega) = G_h(\omega) n_h(\mp\omega)$ .  $n_h(\omega)$  is the average occupation number characterized by the temperature of the bath- $h$ ,  $n_h(\omega) = (e^{\beta_h \omega} - 1)^{-1}$  with  $\beta_h = 1/T_h$  ( $k_B \equiv 1$ ). We assume here the spectral density function of the bath as an Ohmic function with an exponential cutoff:  $G_h(\omega) = \gamma_h \omega e^{-|\omega|/\omega_c}$ , where  $\gamma_h$  is a dimensionless coupling strength and  $\omega_c$  is the cutoff frequency.

Collecting all the 12 terms renders the Redfield master equation. Many time-dependent terms (called the non-secular terms), such as  $\tau_{13} \rho_S \tau_{13} e^{-2i\omega_3 t}$ ,  $\tau_{13} \rho_S \tau_{12} e^{-i(\omega_2+\omega_3)t}$ , and  $\tau_{13} \rho_S \tau_{21} e^{-i(\omega_3-\omega_2)t}$ , then present in Eq. (A9).

We denote by  $t_S$  the timescale of the intrinsic evolution of the system, which is in the same order of a typical value for  $|\omega_m - \omega_n|^{-1}$ ,  $m \neq n$ , involving the energy-spacing

of the system. If  $t_S$  is much larger than the typical timescale of the relaxation time of the system  $t_R \sim \gamma_\mu^{-1}$ ,  $\mu = h, c, w$ , the non-secular terms of rapid oscillation may be safely neglected [36]. Thus the condition of performing a full secular approximation is  $\gamma_\mu \ll |\omega_m - \omega_n|$ .

While in many models as well as ours, although the decay rates are set as  $\gamma_{h,c,w}/\omega_a \sim 0.01$  satisfying Born approximation, the energy level  $\omega_b$  is comparable to  $\omega_a$  in magnitude. Thus the actual condition is  $\omega_2 + \omega_3 \gg \omega_3 - \omega_2 \sim \gamma_{h,c,w}$ . Consequently we have to employ a partial secular approximation by neglecting the rapid-oscillating terms, such as  $e^{-2i\omega_3 t}$  and  $e^{-i(\omega_2+\omega_3)t}$ , but keeping the slow-oscillating terms, such as  $e^{-i(\omega_3-\omega_2)t}$ .

Under the partial secular approximation, Eq. (A9) is thus rewritten as

$$\begin{aligned}
& \text{Tr}_B [H_{SB}^h(t) \rho_S \rho_B H_{SB}^h(t-s)] \\
&= \Gamma_{h3}^+(\omega_3) \tau_{13} \rho_S \tau_{31} + \Gamma_{h1}^+(\omega_3) \tau_{13} \rho_S \tau_{21} e^{-i(\omega_3-\omega_2)t} \\
&+ \Gamma_{h3}^-(\omega_3) \tau_{31} \rho_S \tau_{13} + \Gamma_{h1}^-(\omega_3) \tau_{31} \rho_S \tau_{12} e^{i(\omega_3-\omega_2)t} \\
&+ \Gamma_{h2}^+(\omega_2) \tau_{12} \rho_S \tau_{21} + \Gamma_{h1}^+(\omega_2) \tau_{12} \rho_S \tau_{31} e^{-i(\omega_2-\omega_3)t} \\
&+ \Gamma_{h2}^-(\omega_2) \tau_{21} \rho_S \tau_{12} + \Gamma_{h1}^-(\omega_2) \tau_{21} \rho_S \tau_{13} e^{i(\omega_2-\omega_3)t}.
\end{aligned} \tag{A10}$$

So did all the remaining terms in Eq. (A8). Then after rotating back to the Schrödinger picture, we attain the Redfield master equation with a partial secular approximation as Eq. (7) in the main text.

Following Eq. (7), the dynamical equations of the three-level system with inner coupling in terms of matrix elements are given by

$$\begin{aligned}
\dot{\rho}_{11} &= -2[\Gamma_{h3}^-(\omega_3) + \Gamma_{h2}^-(\omega_2) + \Gamma_{c2}^-(\omega_3) + \Gamma_{c3}^-(\omega_2)]\rho_{11} + 2[\Gamma_{h2}^+(\omega_2) + \Gamma_{c3}^+(\omega_2)]\rho_{22} + 2[\Gamma_{h3}^+(\omega_3) + \Gamma_{c2}^+(\omega_3)]\rho_{33} \\
&+ [\Gamma_{h1}^+(\omega_3) - \Gamma_{c1}^+(\omega_3) + \Gamma_{h1}^-(\omega_2) - \Gamma_{c1}^-(\omega_2)](\rho_{23} + \rho_{32}) \\
\dot{\rho}_{22} &= 2[\Gamma_{h2}^-(\omega_2) + \Gamma_{c3}^-(\omega_2)]\rho_{11} - 2[\Gamma_{h2}^+(\omega_2) + \Gamma_{c3}^+(\omega_2) + \Gamma_w^-(\Omega)]\rho_{22} + 2\Gamma_w^+(\Omega)\rho_{33} - [\Gamma_{h1}^+(\omega_3) - \Gamma_{c1}^+(\omega_3)](\rho_{23} + \rho_{32}) \\
\dot{\rho}_{33} &= 2[\Gamma_{h3}^-(\omega_3) + \Gamma_{c2}^-(\omega_3)]\rho_{11} + 2\Gamma_w^-(\Omega)\rho_{22} - 2[\Gamma_{h3}^+(\omega_3) + \Gamma_{c2}^+(\omega_3) + \Gamma_w^+(\Omega)]\rho_{33} - [\Gamma_{h1}^-(\omega_2) - \Gamma_{c1}^-(\omega_2)](\rho_{23} + \rho_{32}) \\
\dot{\rho}_{23} &= [2i\Omega - \Gamma_{h3}^+(\omega_3) - \Gamma_{c2}^+(\omega_3) - \Gamma_{h2}^-(\omega_2) - \Gamma_{c3}^-(\omega_2) - \Gamma_w^+(\Omega) - \Gamma_w^-(\Omega)]\rho_{23} \\
&+ [\Gamma_{h1}^-(\omega_3) - \Gamma_{c1}^-(\omega_3) + \Gamma_{h1}^-(\omega_2) - \Gamma_{c1}^-(\omega_2)]\rho_{11} - [\Gamma_{h1}^-(\omega_2) - \Gamma_{c1}^-(\omega_2)]\rho_{22} - [\Gamma_{h1}^+(\omega_3) - \Gamma_{c1}^+(\omega_3)]\rho_{33} \\
\dot{\rho}_{32} &= [-2i\Omega - \Gamma_{h3}^+(\omega_3) - \Gamma_{c2}^+(\omega_3) - \Gamma_{h2}^-(\omega_2) - \Gamma_{c3}^-(\omega_2) - \Gamma_w^+(\Omega) - \Gamma_w^-(\Omega)]\rho_{32} \\
&+ [\Gamma_{h1}^-(\omega_3) - \Gamma_{c1}^-(\omega_3) + \Gamma_{h1}^-(\omega_2) - \Gamma_{c1}^-(\omega_2)]\rho_{11} - [\Gamma_{h1}^-(\omega_2) - \Gamma_{c1}^-(\omega_2)]\rho_{22} - [\Gamma_{h1}^+(\omega_3) - \Gamma_{c1}^+(\omega_3)]\rho_{33}.
\end{aligned} \tag{A11}$$

As shown by Eq. (A11), the off-diagonal (coherence) terms  $\rho_{23}$  and  $\rho_{32}$  are closely associated with the diagonal

terms  $\rho_{11}$ ,  $\rho_{22}$  and  $\rho_{33}$ . Thus the steady state obtained by  $\dot{\rho} = 0$  may have residue quantum coherence, which is a mark of quantumness.

- 
- [1] M. O. Scully, M. S. Zubairy, G. S. Agarwal, and H. Walther, *Extracting work from a single heat bath via vanishing quantum coherence*, *Science* **299**, 862 (2003).  
[2] J. Roßnagel, O. Abah, F. Schmidt-Kaler, K. Singer, and

- E. Lutz, *Nanoscale heat engine beyond the carnot limit*, *Phys. Rev. Lett.* **112**, 030602 (2014).  
[3] G. Guarneri, M. Kolář, and R. Filip, *Steady-state coherences by composite system-bath interactions*,

- Phys. Rev. Lett. **121**, 070401 (2018).
- [4] C. Mukhopadhyay, *Generating steady quantum coherence and magic through an autonomous thermodynamic machine by utilizing a spin bath*, Phys. Rev. A **98**, 012102 (2018).
  - [5] M. Kilgour and D. Segal, *Coherence and decoherence in quantum absorption refrigerators*, Phys. Rev. E **98**, 012117 (2018).
  - [6] H. T. Quan, Y.-x. Liu, C. P. Sun, and F. Nori, *Quantum thermodynamic cycles and quantum heat engines*, Phys. Rev. E **76**, 031105 (2007).
  - [7] G. A. Barrios, F. Albarrán-Arriagada, F. A. Cárdenas-López, G. Romero, and J. C. Retamal, *Role of quantum correlations in light-matter quantum heat engines*, Phys. Rev. A **96**, 052119 (2017).
  - [8] K. E. Dorfman, D. Xu, and J. Cao, *Efficiency at maximum power of a laser quantum heat engine enhanced by noise-induced coherence*, Phys. Rev. E **97**, 042120 (2018).
  - [9] M. H. Lee and B. D. Dunietz, *Active control of thermal transport in molecular spin valves*, Phys. Rev. B **88**, 045421 (2013).
  - [10] G. Tang, J. Thingna, and J. Wang, *Thermodynamics of energy, charge, and spin currents in a thermoelectric quantum-dot spin valve*, Phys. Rev. B **97**, 155430 (2018).
  - [11] B. Guo, T. Liu, and C.-s. Yu, *Multifunctional quantum thermal device utilizing three qubits*, Phys. Rev. E **99**, 032112 (2019).
  - [12] A. Levy and R. Kosloff, *Quantum absorption refrigerator*, Phys. Rev. Lett. **108**, 070604 (2012).
  - [13] L. A. Correa, J. P. Palao, D. Alonso, and G. Adesso, *Quantum-enhanced absorption refrigerators*, Sci. Rep. **4**, 3949 (2015).
  - [14] D. Segal, *Current fluctuations in quantum absorption refrigerators*, Phys. Rev. E **97**, 052145 (2018).
  - [15] N. Li, J. Ren, L. Wang, G. Zhang, P. Hänggi, and B. Li, *Colloquium: Phononics: Manipulating heat flow with electronic analogs and beyond*, Rev. Mod. Phys. **84**, 1045 (2012).
  - [16] K. Joulain, J. Drevillon, Y. Ezzahri, and J. Ordonez-Miranda, *Quantum thermal transistor*, Phys. Rev. Lett. **116**, 200601 (2016).
  - [17] P. Erker, M. T. Mitchison, R. Silva, M. P. Woods, N. Brunner, and M. Huber, *Autonomous quantum clocks: Does thermodynamics limit our ability to measure time?* Phys. Rev. X **7**, 031022 (2017).
  - [18] M. Mehboudi, A. Sanpera, and L. A. Correa, *Thermometry in the quantum regime: recent theoretical progress*, J. Phys. A: Math. Theor. **52**, 303001 (2019).
  - [19] G. Kucsko, P. C. Maurer, N. Y. Yao, M. Kubo, H. J. Noh, P. K. Lo, H. Park, and M. D. Lukin, *Nanometre-scale thermometry in a living cell*, Nature **500**, 54 (2013).
  - [20] G. W. Walker, V. C. Sundar, C. M. Rudzinski, A. W. Wun, M. G. Bawendi, and D. G. Nocera, *Quantum-dot optical temperature probes*, Appl. Phys. Lett. **83**, 3555 (2003).
  - [21] M. Zgirski, M. Foltyn, A. Savin, K. Norowski, M. Meschke, and J. Pekola, *Nanosecond thermometry with josephson junctions*, Phys. Rev. Applied **10**, 044068 (2018).
  - [22] S. Jevtic, D. Newman, T. Rudolph, and T. M. Stace, *Single-qubit thermometry*, Phys. Rev. A **91**, 012331 (2015).
  - [23] P. Neumann, I. Jakobi, F. Dolde, C. Burk, R. Reuter, G. Waldherr, J. Honert, T. Wolf, A. Brunner, J. H. Shim, et al., *High-precision nanoscale temperature sensing using single defects in diamond*, Nano Lett. **13**, 2738 (2013).
  - [24] F. Haupt, A. Imamoglu, and M. Kroner, *Single quantum dot as an optical thermometer for millikelvin temperatures*, Phys. Rev. Applied **2**, 024001 (2014).
  - [25] F. Seilmeier, M. Hauck, E. Schubert, G. J. Schinner, S. E. Beavan, and A. Högele, *Optical thermometry of an electron reservoir coupled to a single quantum dot in the millikelvin range*, Phys. Rev. Applied **2**, 024002 (2014).
  - [26] R. Sánchez and M. Büttiker, *Optimal energy quanta to current conversion*, Phys. Rev. B **83**, 085428 (2011).
  - [27] Y. Zhang and J. Chen, *Thermometry based on coulomb-coupled quantum dots*, Physica E **114**, 113635 (2019).
  - [28] J. Yang, C. Elouard, J. Splettstoesser, B. Sothmann, R. Sánchez, and A. N. Jordan, *Thermal transistor and thermometer based on coulomb-coupled conductors*, Phys. Rev. B **100**, 045418 (2019).
  - [29] P. P. Hofer, J. B. Brask, M. Perarnau-Llobet, and N. Brunner, *Quantum thermal machine as a thermometer*, Phys. Rev. Lett. **119**, 090603 (2017).
  - [30] P. P. Hofer, M. Perarnau-Llobet, L. D. M. Miranda, G. Haack, R. Silva, J. B. Brask, and N. Brunner, *Markovian master equations for quantum thermal machines: local versus global approach*, New J. Phys. **19**, 123037 (2017).
  - [31] S. Li, C. Cai, and C. Sun, *Steady quantum coherence in non-equilibrium environment*, Ann. Phys. **360**, 19 (2015).
  - [32] Z. Wang, W. Wu, G. Cui, and J. Wang, *Coherence enhanced quantum metrology in a nonequilibrium optical molecule*, New J. Phys. **20**, 033034 (2018).
  - [33] Y. Huangfu and J. Jing, *Steady bipartite coherence induced by non-equilibrium environment*, Sci. China Phys. Mech. **61**, 010311 (2018).
  - [34] Z. Wang, W. Wu, G. Cui, and J. Wang, *Coherence enhanced quantum metrology in a nonequilibrium optical molecule*, New J. Phys. **20**, 033034 (2018).
  - [35] C. Wang, D. Xu, H. Liu, and X. Gao, *Thermal rectification and heat amplification in a nonequilibrium v-type three-level system*, Phys. Rev. E **99**, 042102 (2019).
  - [36] H. P. Breuer and F. Petruccione, *The theory of open quantum systems*, (Oxford University Press, England, 2002).
  - [37] V. Gorini, A. Kossakowski, and E. C. G. Sudarshan, *Completely positive dynamical semigroups of n-level systems*, J. Math. Phys. **17**, 821 (1976).
  - [38] G. Lindblad, *On the generators of quantum dynamical semigroups*, Commun. Math. Phys. **48**, 119 (1976).
  - [39] D. Farina and V. Giovannetti, *Open-quantum-system dynamics: Recovering positivity of the red-field equation via the partial secular approximation*, Phys. Rev. A **100**, 012107 (2019).
  - [40] M. Cattaneo, G. L. Giorgi, S. Maniscalco, and R. Zambrini, *Local versus global master equation with common and separate baths: superiority of the global approach in partial secular approximation*, New J. Phys. **21**, 113045 (2019).
  - [41] G. L. Yudin, S. Chelkowski, J. Itatani, A. D. Bandrauk, and P. B. Corkum, *Attosecond photoionization of coherently coupled electronic states*, Phys. Rev. A **72**, 051401 (2005).
  - [42] J. E. Geusic, E. O. Schulz-DuBios, and H. E. D.

- Scovil, *Quantum equivalent of the carnot cycle*, *Phys. Rev.* **156**, 343 (1967).
- [43] B. Rutten, M. Esposito, and B. Cleuren, *Reaching optimal efficiencies using nanosized photoelectric devices*, *Phys. Rev. B* **80**, 235122 (2009).
- [44] B. Szukiewicz, U. Eckern, and K. I. Wysokiński, *Optimisation of a three-terminal nonlinear heat nano-engine*, *New J. Phys.* **18**, 023050 (2016).
- [45] J.-H. Jiang and Y. Imry, *Near-field three-terminal thermoelectric heat engine*, *Phys. Rev. B* **97**, 125422 (2018).
- [46] J. R. Prance, C. G. Smith, J. P. Griffiths, S. J. Chorley, D. Anderson, G. A. C. Jones, I. Farrer, and D. A. Ritchie, *Electronic refrigeration of a two-dimensional electron gas*, *Phys. Rev. Lett.* **102**, 146602 (2009).
- [47] Y. Zhang, G. Lin, and J. Chen, *Three-terminal quantum-dot refrigerators*, *Phys. Rev. E* **91**, 052118 (2015).
- [48] J. V. Koski, A. Kutvonen, I. M. Khaymovich, T. Ala-Nissila, and J. P. Pekola, *On-chip maxwell's demon as an information-powered refrigerator*, *Phys. Rev. Lett.* **115**, 260602 (2015).
- [49] P. A. Erdman, B. Bhandari, R. Fazio, J. P. Pekola, and F. Taddei, *Absorption refrigerators based on coulomb-coupled single-electron systems*, *Phys. Rev. B* **98**, 045433 (2018).
- [50] A.-M. Daré, *Comparative study of heat-driven and power-driven refrigerators with coulomb-coupled quantum dots*, *Phys. Rev. B* **100**, 195427 (2019).
- [51] N. Walldorf, A.-P. Jauho, and K. Kaasbjerg, *Thermoelectrics in coulomb-coupled quantum dots: Cotunneling and energy-dependent lead couplings*, *Phys. Rev. B* **96**, 115415 (2017).
- [52] H. Thierschmann, R. Sánchez, B. Sothmann, F. Arnold, C. Heyn, W. Hansen, H. Buhmann, and L. W. Molenkamp, *Three-terminal energy harvester with coupled quantum dots*, *Nat. Nanotechnology* **10**, 854 (2015).
- [53] P. Strasberg, G. Schaller, T. L. Schmidt, and M. Esposito, *Fermionic reaction coordinates and their application to an autonomous maxwell demon in the strong-coupling regime*, *Phys. Rev. B* **97**, 205405 (2018).
- [54] M. Galperin and A. Nitzan, *Current-induced light emission and light-induced current in molecular-tunneling junctions*, *Phys. Rev. Lett.* **95**, 206802 (2005).
- [55] M. Galperin and A. Nitzan, *Optical properties of current carrying molecular wires*, *J. Chem. Phys.* **124**, 234709 (2006).
- [56] Y. Zhang, Z. Yang, X. Zhang, B. Lin, G. Lin, and J. Chen, *Coulomb-coupled quantum-dot thermal transistors*, *EPL* **122**, 17002 (2018).